An efficient strategy for determining intensity-based range variances of terrestrial laser scanners for rigorous deformation analyses

Omar ABDELGAFAR[1,*], **Selin PALAZ**[1], **Yihui YANG**[1], and **Christoph HOLST**[1]

[1] *Chair of Engineering Geodesy, TUM School of Engineering and Design, Technical University of Munich, Germany , (o.abdelgafar, selin.palaz, yihui.yang, christoph.holst)@tum.de*

[*] *corresponding author*

Abstract

The fast improvement of laser scanning technology has pushed terrestrial laser scanning (TLS) to the forefront of geodetic deformation analysis. As TLS becomes more integrated into this field, it is critical to construct a stochastic model that appropriately describes the uncertainty in TLS measurements. This includes creating a valid and fully populated variance-covariance matrix (VCM) for TLS polar observations. This approach requires estimating variances for range, vertical, and horizontal angles, as well as determining the correlations between these observations. In this contribution, we present an efficient strategy to determine the range variances in TLS based on raw intensities. A two-dimensional measuring approach is used on various specimens with TLS devices that offer raw intensity measurements, such as the Z+F Imager 5016A series. Verification is carried out using the observations from real-world scenarios (Brucher Water Dam and Bonn reference wall). Overall, this work proposes a methodology for evaluating the range variations of the specified TLS device.

Keywords: TLS, Stochastic Model, Variance Propagation, Uncertainty, Random Errors, Point Clouds

1 Introduction

Terrestrial Laser Scanners (TLS) represent an important technological advancement in present geodetic research and applications, facilitating the acquisition of 3D point clouds with high precision and spatial resolution. Recent developments in laser technology and data processing algorithms have upgraded their capabilities, allowing for the generation of dense point clouds on complex surfaces (Li et al., 2021) and built structures (Zhou et al., 2024).

These advancements have reinforced using TLS in geodetic engineering, particularly for applications that require millimeter-level of accuracy (Holst and Kuhlmann, 2016): e.g., deformation monitoring and structural analysis of critical infrastructure such as water dams (Kerekes and Schwieger, 2021), radio telescopes (Holst et al., 2017), and bridges (Zhou et al., 2024). Distinguishing between actual deformation and measurement uncertainty is of paramount importance for all these applications.

The TLS output is represented as a discrete point cloud defined by local Cartesian coordinates and backscattered intensity. However, the raw measurements of the TLS are originally polar, consisting of ranges from the scanner to the scanning target, vertical angles, and horizontal angles. The uncertainty of these measurements arises from four primary error sources: scanner imperfections, atmospheric conditions, scanning geometry, and the physical properties of the scanned surface (Soudarissanane et al., 2011). Thus, a comprehensive understanding of TLS stochastic behavior necessitates the development of a fully populated variance-covariance matrix (VCM) for the raw measurements.

The construction of the VCM requires a representation of variances and the covariances of these polar measurements. Most studies focus only on the estimation of the range variances. For example, the first physical relation between the rage standard deviation and the backscattered intensity was introduced by Wujanz et al. (2017), which led to an intensity-based variance model for TLS range measurements applying 1D measuring mode. Afterward, Wujanz et al. (2018) employed 3D scanning mode, estimating range noise from best-fitting planes. Besides,

Heinz et al. (2018) estimated intensity-based variance model for 2D laser scanners, using repetitive profile scanning.

Reviewing these studies reveals that range variance estimation has been conducted in controlled laboratory environments with specialized specimens, as well as experimental configurations like rail-bound comparator tracks, which inherently limit the applicability of these methods. To address these limitations, this study aims to make the following two main contributions:

- We introduce a workflow that enables high-end 3D laser scanner users to estimate range variances for the scanned objects based on a 2D scanning mode.
- We evaluate this workflow's effectiveness when applied to high-end laser scanners using raw intensity data.

This workflow consists of a measurement concept and data processing strategy. We will introduce it in Section 3 and 4 and validate it in Section 5

2 State of the art

As with any geodetic instrument, TLS measurements are affected by both systematic and random errors due to different error sources (Soudarissanane et al., 2011). The scanner imperfections, such as misalignments or eccentricities, mostly lead to systematic errors. Although calibration procedures deal with most of these errors, the remaining errors that are considered random are due to variability in calibration parameters and their sensitivity to temporal and environmental conditions (Medic et al., 2020).

Additionally, atmospheric effects due to variations in temperature, air pressure, and humidity influence the propagation characteristics of the laser beam. These refraction-induced systematic errors can be reduced by developing correction models based on additional meteorological data (Friedli et al., 2019). However, the randomized residuals that exacerbate with increasing measurement range vary slowly in both time and space in stable atmospheric conditions. Also, random errors can occur due to high atmospheric fluctuations (Kerekes and Schwieger, 2021).

Furthermore, both scanning geometry and surface properties affect the measurement accuracy randomly and systematically, depending on factors such as reflectivity, surface interaction, and scanning angles. Among these, systematic errors often dominate and arise from the interaction between the laser beam and the scanned surface (Soudarissanane et al., 2011; Zámečníková et al., 2014).

All of these error sources affect the range and angular measurements of the TLS while also introducing correlations between observations. Consequently, a comprehensive understanding of TLS stochastic behavior requires the development of a fully populated VCM, as the major component of uncertainty is random. Anyhow, as stated in the introduction, this study focuses only on the range variances as an initial entry for the VCM.

Wujanz et al. (2017) proposed a strategy for empirically estimating range variances σ_r^2 of laser scanner measurements, which characterizes the relationship between range noise and backscattered intensity through an exponential function:

$$\sigma_r = aI^b + c. \tag{1}$$

where σ_r represents the range standard deviation, I is the backscattered intensity, and a, b, and c are the intensity-based range variance parameters.

Equation 1 takes into account variations of intensity as well as range variance due to the object distances, the variations in incidence angles, and the radiometric properties of the scanned surface. However, the methodology for estimating the parameters a, b, c introduced by Wujanz et al. (2017) relied on the 1D scanning mode, which involves repeated single-point measurements at varying distances. This approach is not freely usable due to safety concerns associated with the concentrated energy of the laser.

To address the limitations of the 1D mode, Hobiger et al. (2018); Wujanz et al. (2018); Schmitz et al. (2019) employed the standard 3D scanning mode to investigate range noise empirically. Their methodology estimated residuals from best-fitting planes that derived from the point cloud of planar targets, which were oriented to achieve zero incidence angles and minimize angular encoder deviations. However, it relied on specific model assumptions that do not fit targets with non-uniform

backscattering. Thus, those methods are only applicable for special setups.

Based on the mentioned methodologies, Heinz et al. (2018) introduced a strategy for deriving intensity-based range variances suitable for 2D laser scanners, i.e. profile laser scanners, specifically the Z+F Profiler 9012A. Following this method, Schill et al. (2024) introduced applying this method using 3D high-end laser scanners. This method relies on repetitive profile scanning in order to estimate range uncertainties without the need for any geometric primitive assumptions.

This summary shows that strategies for determining intensity-based range variances for TLS are manifold. Anyhow, they still suffer from the complexity of the measurement setup and the necessity of special specimens, as previous strategies were performed in controlled environments. In contrast, the introduced workflow enables scanner users to estimate range uncertainties under normal conditions using the scanning target itself to build the intensity-based range variance model. This is why we implemented a new workflow, as presented in this study.

3 Measurement concept

Laser scanner manufacturers either offer to directly export the raw intensity values or scale them before the user is offered to export them. Sometimes, both options exist. This paper focuses on scanners that provide raw intensity values, specifically the Z+F Imager 5016A (Zoller + Fröhlich GmbH, 2025a). This scanner is also capable of operating in both panoramic (3D) and profile (2D) modes, supporting various scanning rates across both dimensions. Considering the measurement efficiency, we adopt the 2D method to derive an intensity-based range variance model herein.

As estimating range standard deviations for fitting Equation 1 requires data redundancy, the measurement concept employed involved profile scanning of the target at close, medium, and long ranges using a scanning rate of 1.09 MHz. Consequently, we can cover all range variations as well as the targeted intensity spectrum.

Based on that, in this section, we introduce a measurement concept to construct the model. The experiment was divided into two phases. The first phase aimed to construct the intensity-based range variance model in a controlled laboratory environment using a spectralon board (Figure 1). The second phase sought to estimate the same model under real-world conditions, observing natural objects such as the Brucher water dam in Bonn (Figure 2) and the Bonn reference wall (Figure 3).

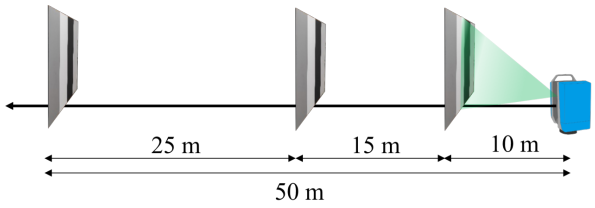

Figure 1. Measurement configuration using Spectralon Board with four colors (dark gray, white, black, light gray) observed by the TLS in profile mode at $10m$, $25m$, and $50m$ distance

In the first phase, the scanner remained stationary while the spectralon board with four colors that varied from the white color representing a high-intensity reflectivity to the black one with a very low reflectivity was positioned at three distances: $10m$, $25m$, and $50m$ (Figure 1). For each color of the board, at least 3,000 profile lines were recorded to have a sufficient number of points for each target. Hence, we can cover the full intensity spectrum for all the ranges.

Conversely, in the second phase, we aimed to evaluate our workflow; therefore, profile scanning of two lines on each side of the Brucher water dam (Figure 2) and the Bonn reference wall (Figure 3) was conducted at distances of $10m$, $20m$, and $30m$.

4 Data Processing

This chapter provides an overview of the data processing to build the intensity-based range variance model. To achieve our goal, as shown in Figure 4, the data processing step is structured into two stages: Preprocessing and model fitting.

4.1 Data Preprocessing

In this step, we aim to prepare the data for the subsequent model fitting procedure. This starts by exporting the raw data from the scanner using the manufacturer software *Laser Control* (Zoller + Fröhlich GmbH, 2025b), which allows us to export the polar

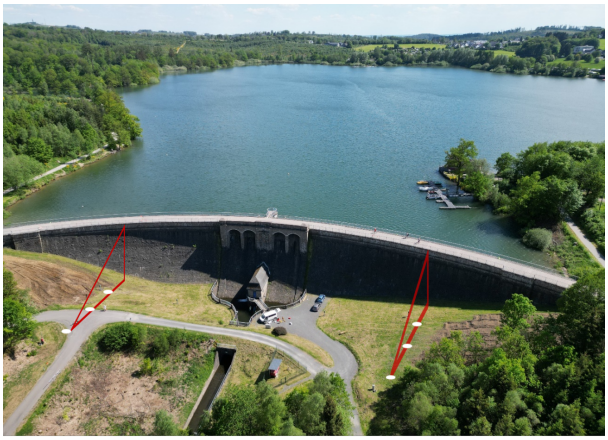

Figure 2. Measurement setup at the Brucher water dam, where two scanning lines were placed on each side at distances of 10 m, 20 m, and 30 m, represented by white points.

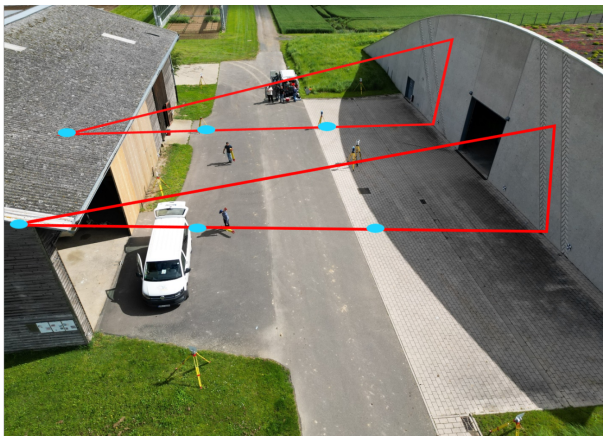

Figure 3. Measurement configuration at the Bonn reference wall, illustrating two scanning lines on each side positioned at 10 m, 20 m, and 30 m, marked by blue points.

measurements of profile scanning.

After exporting the data, outliers in the range and intensity values are identified and removed. To achieve this, the range and intensity values are first grouped according to vertical ticks across all profiles of the target. In turn, for each vertical tick, a series of range values and their corresponding intensity values are obtained.

To assess variability within each vertical tick, the standard deviation is estimated relative to both the mean and the median for both the range r and intensity values I (marked as x in the subsequent equations). The standard deviation concerning the mean

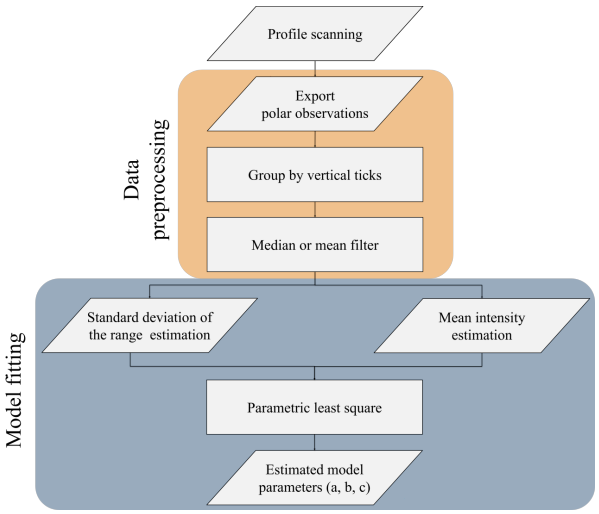

Figure 4. Schematic representation of the data processing workflow.

is defined as

$$\sigma_{\text{mean}} = \sqrt{\frac{1}{n-1}\sum_{i=1}^{n}(x_i - \bar{x})^2}, \tag{2}$$

where $\bar{x}$ is the arithmetic mean:

$$\bar{x} = \frac{1}{n}\sum_{i=1}^{n} x_i \tag{3}$$

Similarly, the standard deviation for the median is given by

$$\sigma_{\text{median}} = \sqrt{\frac{1}{n-1}\sum_{i=1}^{n}(x_i - \text{median}(x))^2}, \tag{4}$$

where $\text{median}(x)$ denotes the median of the data set.

Outlier removal is performed by applying a threshold based on three times the standard deviation relative to the mean or the median. The measurement x_i is considered an outlier if either of the following conditions is met:

$$|x_i - \bar{x}| > 3\sigma_{\text{mean}}, \tag{5}$$

$$|x_i - \text{median}(x)| > 3\sigma_{\text{median}}. \tag{6}$$

All observations satisfying this condition are removed from the vertical tick group, ensuring that only values within an acceptable range are retained.

4.2 Model fitting

Once the outliers are removed, we can estimate the mean intensity using Equation 3 and the standard

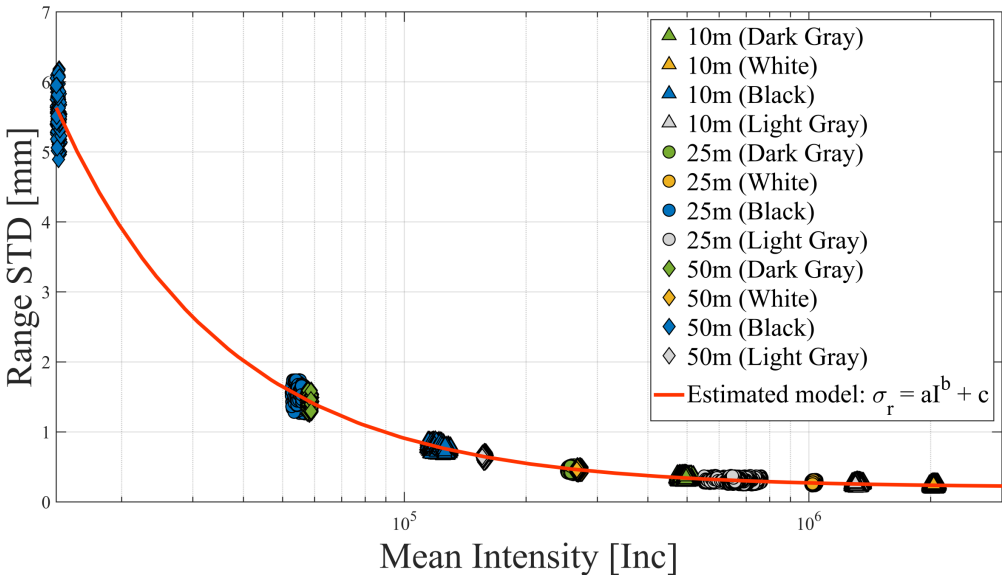

Figure 5. Mean intensity and range standard deviation (STD) for each vertical tick on the Spectralon board (dark gray, white, black, and light gray) at 10 m, 25 m, and 50 m following data preprocessing, along with the intensity-based range variance model of the Z+F Imager 5016A at a 1.09 MHz scanning rate after parameter estimation.

deviation of the range per tick using Equation 2. Applying these computations to each scanning data set for each color of the spectralon board, we obtain filtered points that have a mean intensity and a range standard deviation (Figure 5).

As Figure 5 illustrates, the data exhibits the characteristics of the intensity-based range variance model (Equation 1). Consequently, this dataset is utilized to estimate the model parameters a, b, c (Table 1) for the 1.09 MHz scanning rate using parametric least squares.

The relationship between mean intensity values and range uncertainties, constructed after data processing, shows that targets with low intensities observed from long ranges have high range uncertainties, while targets with high intensities and short ranges have lower uncertainties. Additionally, a single model represents the intensity-based range variance across close, medium, and long ranges.

Table 1. Intensity-based range variance model parameters of the Z+F Imager 5016A at a 1.09 MHz scanning rate.

Scanning Rate	$\hat{\mathbf{a}}\left[\frac{\mathbf{mm}}{\mathbf{Inc}}\right]$	$\hat{\mathbf{b}}\,[-]$	$\hat{\mathbf{c}}\,[\mathbf{mm}]$
1.09 MHz	100195	-1.031	0.21

5 Model Validation

We validate the results using two approaches. The first approach involves cross-validation with the Brucher water dam and Bonn reference wall datasets. The second approach examines whether the model could be independently derived from each of those datasets. If feasible, the model obtained from laboratory observations could then be compared with those estimated from the water dam and reference wall datasets.

5.1 Cross-Validation

To evaluate the model's accuracy, cross-validation is performed using the Brucher water dam and Bonn reference wall datasets. After exporting each dataset, outlier removal is applied as in Section 4.1. Consequently, we estimate both the mean intensity, $\bar{I}_{Env}$, and the standard deviation, $\hat{\sigma}_{r,Env}$, for each vertical tick. For the same mean intensity values, we generate the corresponding range standard deviations, $\sigma_{r,Lab}$, but this time from the intensity-based range variance model generated in the laboratory. The residuals, ε_i, are then computed as the difference between the model-predicted range standard deviation, $\sigma_{r,Lab}$, and the estimated standard deviation, $\hat{\sigma}_{r,Env}$.

To estimate the accuracy of the model, we cal-

culate the root mean square error (RMSE) as the arithmetic mean of the squared residual ε_i for both datasets, which are presented in Table 2. From this table, the RMSE values between the model estimated from the Bonn reference wall dataset and the Spectralon board are lower than those between the Brucher water dam dataset and the Spectralon board. This is due to the higher uncertainty of the water dam dataset, influenced by its geometry and surface properties.

Table 2. RMSE of the intensity-based range variance model fitting at 1.09 MHz, evaluated on the Brucher water dam and Bonn reference wall datasets.

Target	**RMSE [mm]**
Bonn reference wall	0.03
Brucher water dam	0.07

5.2 Model Comparison

In the preceding section, range standard deviations and mean intensities for the Brucher water dam and Bonn reference wall datasets were estimated. Plotting these values against the intensity-based range variance model in Figure 6 shows that the data distribution follows a similar trend to the estimated model. This observation motivated the assessment of whether individually fitted models could be derived for each dataset separately.

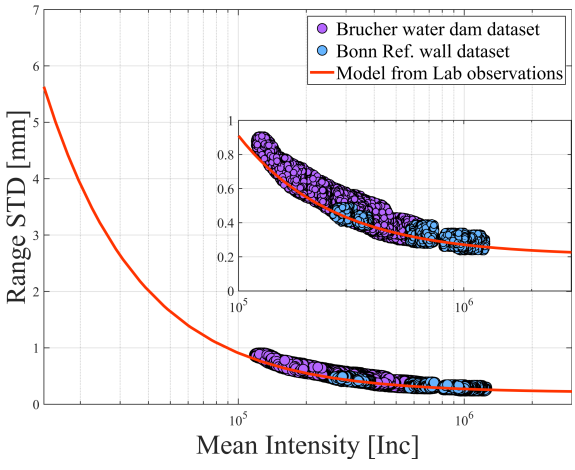

Figure 6. The Brucher water dam and Bonn reference wall datasets behavior comparing with the intensity-based range variance model of the same scanning rate (1.09MHz).

By applying the parametric least squares adjustment, as described in Section 4.2, the parameters for each function are estimated (Table 3). Comparing the two sets of model parameters, the Brucher water dam dataset has higher overall uncertainty than

Table 3. Estimated parameters for the intensity-based range variance model using the Bonn Reference Wall and Brucher Water Dam datasets.

Dataset	$\hat{\mathbf{a}}\left[\frac{\mathbf{mm}}{\mathbf{Inc}}\right]$	$\hat{\mathbf{b}}\,[-]$	$\hat{\mathbf{c}}\,[\mathbf{mm}]$
Bonn Reference Wall	4386	-0.775	0.19
Brucher Water Dam	18516	-0.872	0.18

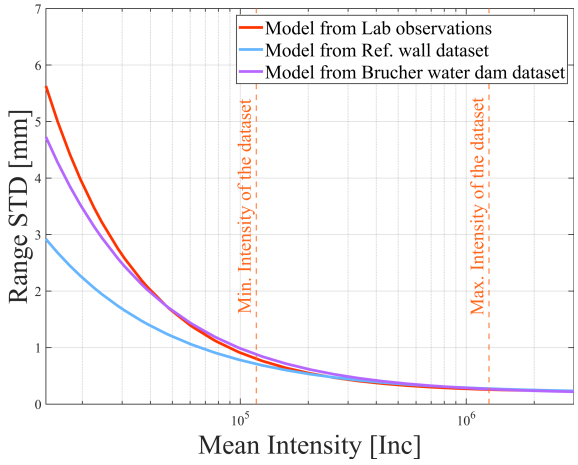

Figure 7. Comparison of intensity-based range variance models derived from the Spectralon board, Bonn reference wall, and Brucher water dam datasets.

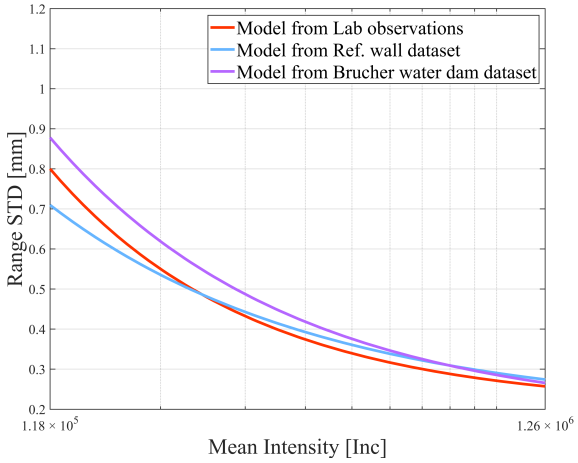

Figure 8. Intensity-based range variance models from the Spectralon board, Bonn reference wall, and Brucher water dam datasets, focusing on the intensity spectrum covered by the Brucher water dam and Bonn reference wall datasets.

the Bonn reference wall dataset, explaining the difference in their a parameters. Parameters a and b generally show large differences compared with Table 1, while parameter c is very close in magnitude. The differences between these parameters will be explained based on the corresponding graphs.

Figure 7 displays the function graphs based upon the lab estimation (Table 1), water dam and reference wall estimation (both in Table 3) over the full range of intensity values, while Figure 8 focuses the same graphs on the limited intensity spectrum that is covered by water dam and reference wall (also highlighted by orange vertical lines in Figure 7). On the one hand, we observe in Figure 8 that the differences between the models are less than 0.2 mm, where the maximal difference is gained for low intensities. On the other hand, Figure 7 implies that the differences can reach up to about 3 mm for low intensities if we consider the full range of possible intensity values. This is clearly an extrapolation effect due to the lack of low-intensity observations.

Once the two models are derived, their validity can be assessed by comparing them against the existing model. This validation is performed by estimating the residuals between the range standard deviation obtained from the model of either the Brucher water dam or the Bonn reference wall and those derived from the model generated using the Spectralon board. Subsequently, the RMSE values were estimated to quantify the deviations, as presented in Table 4.

Table 4. The RMSE values are estimated by computing the residuals between the model estimated from the Spectralon board and the model from the Brucher water dam and Bonn reference wall datasets.

Target	**RMSE** [**mm**]
Bonn reference wall	0.02
Brucher water dam	0.07

As illustrated in Figure 8, the models derived from the two datasets do not have the same behavior compared to the model estimated from the Spectralon board. This variation is due to each target's surface properties. The reference wall has a smooth and uniform surface, while the Brucher water dam exhibits a more complex structure with a concave shape, therefore increasing range measurement uncertainties. This also explains the RMSE values presented in Table 2 and Table 4, where the RMSE estimated using the water dam dataset is higher than that of the reference wall.

6 Conclusion

This article introduces a workflow for calculating intensity-based range variances of TLS using the Z+F Imager 5016A laser scanner. The method was originally tested in a controlled laboratory setting, using a Spectralon board with four distinct intensity levels to calculate range standard deviations and mean intensities at varied distances.

The estimated model has been verified using cross-validation, which compared the estimated range standard deviations from the Brucher water dam and Bonn reference wall datasets to those obtained from the Spectralon-based model. The Bonn reference wall dataset shows fewer deviations because of its smooth and uniform surface, while the Brucher water dam dataset shows higher uncertainties considering its concave geometry and high surface roughness.

The estimated parameters of the intensity-based model reflect variations with distinct a, b, and c values for each dataset, confirming the feasibility of deriving stochastic models without a controlled laboratory setup. However, extending the water dam and reference wall models beyond the intensity coverage range leads to extrapolation, with differences of around 1 mm and 3 mm compared to the Spectralon model. As shown in Figure 7 and Figure 8, these differences are negligible within the covered intensity spectrum, indicating that each model is only valid for its respective surface properties and cannot be generalized for a full intensity range.

Future work will focus on extending this workflow to all available scanning rates of the Z+F Imager 5016A to assess the consistency of the derived stochastic models across different acquisition settings. Additionally, this methodology will be applied to include laser scanners that provide scaled intensity values.

Funding

This research was funded by German Research Foundation (DFG) under grant number 490989047,

DFG FOR 5455 "TLS-Defo".

References

Friedli, E., Presl, R., and Wieser, A. (2019). Influence of atmospheric refraction on terrestrial laser scanning at long range. *Proceedings of the 4th Joint International Symposium on Deformation Monitoring (JISDM), Athens, Greece*.

Heinz, E., Mettenleiter, M., Kuhlmann, H., and Holst, C. (2018). Strategy for Determining the Stochastic Distance Characteristics of the 2D Laser Scanner Z + F Profiler 9012A with Special Focus on the Close Range. *Sensors*, 18(7):2253.

Hobiger, T., Belton, D., and Helmholz, P. (2018). Empirical investigation of a Stochastic model based on intensity values for terrestrial laser scanning. *AVN Allgemeine Vermessungs-Nachrichten*, 125:43–52.

Holst, C. and Kuhlmann, H. (2016). Challenges and present fields of action at laser scanner based deformation analyses. *Journal of Applied Geodesy*, 10(1):17–25.

Holst, C., Schunck, D., Nothnagel, A., Haas, R., Wennerbäck, L., Olofsson, H., Hammargren, R., and Kuhlmann, H. (2017). Terrestrial Laser Scanner Two-Face Measurements for Analyzing the Elevation-Dependent Deformation of the Onsala Space Observatory 20-m Radio Telescope's Main Reflector in a Bundle Adjustment. *Sensors (Basel)*, 17(8):1833.

Kerekes, G. and Schwieger, V. (2021). Determining Variance-Covariance Matrices for Terrestrial Laser Scans: A Case Study of the Arch Dam Kops. In Kopáčik, A., Kyrinovič, P., Erdélyi, J., Paar, R., and Marendić, A., editors, *Contributions to International Conferences on Engineering Surveying*, pages 57–68, Cham. Springer International Publishing.

Li, Y., Liu, P., Li, H., and Huang, F. (2021). A Comparison Method for 3D Laser Point Clouds in Displacement Change Detection for Arch Dams. *ISPRS International Journal of Geo-Information*, 10(3):184. Number: 3 Publisher: Multidisciplinary Digital Publishing Institute.

Medic, T., Holst, C., and Kuhlmann, H. (2020). Optimizing the Target-based Calibration Procedure of Terrestrial Laser Scanners. *Allgemeine Vermessungs-Nachrichten : AVN ; Zeitschrift für alle Bereiche der Geodäsie und Geoinformation*.

Schill, F., Holst, C., Wujanz, D., Hartmann, J., and Paffenholz, J.-A. (2024). Intensity-based stochastic model of terrestrial laser scanners: Methodological workflow, empirical derivation and practical benefit. *ISPRS Open Journal of Photogrammetry and Remote Sensing*, 15:100079.

Schmitz, B., Holst, C., Medic, T., Lichti, D. D., and Kuhlmann, H. (2019). How to Efficiently Determine the Range Precision of 3D Terrestrial Laser Scanners. *Sensors*, 19(6):1466. Number: 6 Publisher: Multidisciplinary Digital Publishing Institute.

Soudarissanane, S., Lindenbergh, R., Menenti, M., and Teunissen, P. (2011). Scanning geometry: Influencing factor on the quality of terrestrial laser scanning points. *ISPRS Journal of Photogrammetry and Remote Sensing*, 66(4):389–399.

Wujanz, D., Burger, M., Mettenleiter, M., and Neitzel, F. (2017). An intensity-based stochastic model for terrestrial laser scanners. *ISPRS Journal of Photogrammetry and Remote Sensing*, 125:146–155.

Wujanz, D., Burger, M., Tschirschwitz, F., Nietzschmann, T., Neitzel, F., and Kersten, T. (2018). *Bestimmung von intensitätsbasierten stochastischen Modellen für terrestrische Laserscanner basierend auf 3D-Punktwolken*.

Zhou, Y., Zhu, J., Lidu, Z., Hu, G., Xin, J., Zhang, H., and Yang, J. (2024). High-Precision Monitoring Method for Bridge Deformation Measurement and Error Analysis Based on Terrestrial Laser Scanning. *Remote Sensing*, 16.

Zoller + Fröhlich GmbH (2025a). Z+F IMAGER® 5016A. Accessed: 2025-02-08.

Zoller + Fröhlich GmbH (2025b). Z+f lasercontrol® software. Accessed: February 10, 2025.

Zámečníková, M., Wieser, A., Woschitz, H., and Ressl, C. (2014). Influence of surface reflectivity on reflectorless electronic distance measurement and terrestrial laser scanning. *Journal of Applied Geodesy*, 8(4):311–326. Publisher: De Gruyter.